CHAPTER 2.4

THE THEORY OF CENTRAL NERVOUS SYSTEM RECORDING

Shy Shoham[1] and Srikantan Nagarajan[2]
[1] *Department of Molecular Biology, Princeton University, Princeton, NJ, 08544*
[2] *Department of Radiology. University of California, San Francisco*
E-mail: sshoham@princeton.edu, sri@radiology.ucsf.edu

A large number of biophysical models and quantitative methods are relevant to the design of Brain-Computer Interfaces and other neuroprosthetic devices that rely on recording neural activity in the CNS. These models describe different biological processes occurring across a range of scales. Here we focus on three that appear most relevant to the neural engineer. At the smallest scale we review models of extracellular potential spread around a spiking neuron as they relate to the sources of signal and noise encountered during microelectrode recordings. We overview a variety of signal detection and pattern recognition methods used in an attempt to reliably and automatically detect single unit activity from these recordings. Next, we look at the way the activity of very large populations of neurons aggregates to form the fields measured using far-field recordings from the skull or scalp. We conclude with a review of the representation of dynamic sensory and motor quantities in the activity of spiking neurons and small populations of neurons within the framework of encoding models and decoding methods.

1. Introduction

A number of neuroprosthetic devices currently under development rely on the ability to record neural activity in the central nervous system either directly using implanted electrode arrays or indirectly from the scalp. These devices include a variety of Brain-Computer Interfaces providing a control and communication interface to paralyzed individuals (see Chapters 7.8 & 7.9) as well as systems for predicting epileptic seizures that are intended to be a part of closed-loop systems for seizure control. Modern procedures for the implantation of deep brain stimulators and other aspects of 'functional neurosurgery' also rely on recording the activity of local neural populations during the selection of intervention sites. In addition, the neural engineer developing a neuroprosthetic device will often rely on recordings of evoked activity in the CNS when seeking an objective evaluation of the function of sensory substitutes like auditory or vision prostheses. These applications as well as other emerging applications are but a

small fraction of the full scope of CNS recording applications in other fields spanning the full spectrum from basic to clinical neuroscience.

Many similarities exist between near-field CNS measurements and techniques used for peripheral nervous system that are described in Chapter 2.2. Typical near-field extracellular measurements are performed by amplifying the potential difference between the microelectrode tip and a reference electrode located within a few millimeters. These recordings are usually broken into two components with widely different experimental significance. The Local Field Potential (LFP) corresponds to coherent low frequency changes in membrane potential (<300 Hz) associated with synaptic currents as well as other sources in cell aggregates, while the higher frequency signal (300–10 kHz) consists mostly of multi-unit activity resulting from action potentials in nearby neurons. The different frequency components represent signals with widely different spatial extent: up to 100 μm for the single-unit signals, several hundreds of microns for the multi-unit signals, and several millimeters for the LFP. This is a result both of the frequency low-pass by neural tissue (simplistically, a lumped RC circuit), and of tighter spatial correlations appearing in the activity in certain lower-frequency bands.

In addition far-field measurements of electric potentials are also routinely performed sub-durally or on the scalp. Sub-dural recordings are also often referred to as electrocorticograms (EcoG) and scalp-recordings as electroencephalography (EEG). Additionally, magnetic field recordings can also be measured on the scalp using magnetoencephalography (MEG). These far-field electrical recordings are similar to LFP in that they only contain significant low-frequency components. However, due to the attenuation by the skull and scalp and spatial filtering by volume-conduction in the brain, the spatial resolution of these recordings is considerably poorer than near-field recordings.

Techniques for measuring surface potentials and extracellular measurements of single-neurons with microelectrodes were developed in 1920s by Berger and Adrian, respectively. Electrode technology for applied as well as basic neuroscience applications has significantly improved over recent years, and much effort is going presently into the development of chronic neural interfaces that will combine high-throughput, good signal to noise ratio, simplicity, reliability and biocompatibility.

2. Extracellular Recording of Action Potentials

Extracellular recordings of neural activity using a single recording microelectrode[53,77] can provide a noisy measurement of action potentials produced by a small number of neurons adjacent to the electrode tip. During an action potential, different parts of neuron's membrane become depolarized leading to a flow of current both inside and outside the neuron. Since the extracellular space is conducting as well, a time-varying potential gradient is formed in the extracellular volume and a potential difference can be measured between a point near the cell and a distant reference location.

A simplified model (Fig. 1) can provide valuable qualitative insights regarding the extracellular potential near a polarized cell[41,48]. At the early part of the action potential, illustrated in the figure, the initial segment of the axon is depolarizing (that is, current is flowing into the cell). Since charge is conserved (only membrane conductance is changing), current loops are established both inside and outside the cell. Since extracellular current is flowing from the surrounding space towards the axon's initial segment that area will have a negative potential, and a similar argument illustrates that the space outside the apical dendrite will be have a positive potential. It is therefore clear that the potential around the neuron behaves approximately like a dipole potential. At later time points the depolarizing region (the current "sink") splits[95] – the one in front propagates forward through the axon (anterograde), and a second moves backwards towards the soma and then into the dendrite (retrograde propagation). A similar diagram can be drawn for other time points with a different arrangement of sources and sinks. As a first approximation the potential dipole is now translating and rotating, as has been observed by a number of experimental studies[79]. More generally, the distribution of sources and sinks becomes fairly complex as the action potential continues to propagate, leading to a complex configuration of extracellular potentials. In fact, it is possible for the potential to be negative near a current source and vice versa for sinks[74].

The simplified model can also be used to derive an approximate relation between the time course of extracellular and membrane potentials (V_{ext} and V_m). Since the extracellular volume is assumed to be resistive, the extracellular potential will be roughly proportional to the current across the membrane. The membrane behaves approximately as an RC circuit, and for transients much shorter than the membrane time constant, current flows primarily through the membrane capacitor. As a result:

$$V_{ext} \propto I_m \propto \frac{dV_m}{dt} \tag{1}$$

This relation has been observed experimentally to hold approximately during combined intra- and extracellular measurements in CNS neurons[37,60]. Clearly, the relationship may fail later in the action potential as the configuration of sources and sinks shifts around. Nevertheless, the fact that a relationship between the intra- and extracellular waveforms does exist is quite useful experimentally. One application of this relationship is the classification of pyramidal neurons versus inter-neurons using the extracellular waveforms. Several studies[62,75] have established that the waveforms produced by interneurons are significantly shorter (<<1 ms) and that waveforms belonging to the two neural populations can be separated with high fidelity using the waveform width.

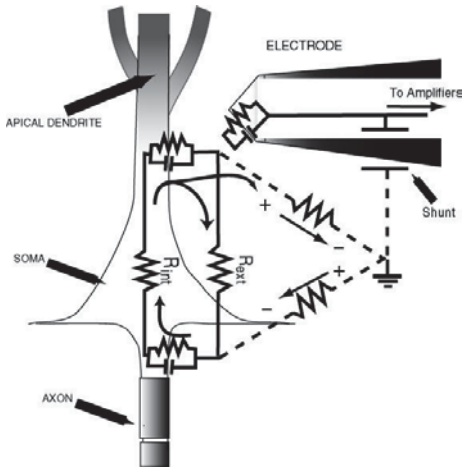

Fig. 1. A schematic representation of the distribution of currents and potential around a pyramidal neuron during the early part of an action potential (basal dendrite not shown). The current sink is near the depolarization in the axon's initial segment, while the dendrites act as passive sources. A highly simplified microelectrode is presented consisting of an RC interface and a shunt.

Approximate qualitative arguments can also be made regarding the impact of the microelectrode impedance on its recording capability[53,77]. We can think of a voltage divider formed by the impedance of the electrode-tissue interface and the electrode shunt (Fig. 1). Decreasing the interface impedance or increasing the shunt impedance results in an increase in the measured signal[23]. Decreasing the input impedance will also reduce the thermal noise. Since the interface impedance is inversely proportional to uninsulated electrode area, it follows that increasing this area will result in a measurable signal from more neurons, which is why lower impedance electrodes are considered 'multi-unit'.

Theoretical calculations of the detailed spatiotemporal evolution of the extracellular potential around a spiking neuron have been outlined by a small number of studies. The neurons in these studies were modeled using multi-compartment models with a variable level of detail and current spread in and between the compartments was calculated using standard cable theory[52]. Specific examples include Rall's calculation of the fields around a simplified motor neuron with seven dendrites and no axon[74] and a related model with a 14 compartment equivalent dendrite[23]. In a recent study by Holt and Koch[40], current flow was calculated for a highly detailed simulated cortical pyramidal neuron using the Neuron simulation environment[38], and used to calculate the extracellular potential.

To calculate the spread of extracellular potential these studies assumed that the extracellular space behaves as a homogenous volume conductor. Under quasi-static conditions, the potential Φ in the homogenous volume conductor behaves according to the Poisson equation:

$$\nabla^2 \Phi = 0 \tag{2}$$

With the following boundary conditions on the membrane:

$$\nabla\Phi = \vec{J}/\sigma \tag{3}$$

Where $\vec{J}$ represents the current sources and σ is the extracellular conductivity.

Interestingly, these equations are the same as those obtained in electrostatics if one were to replace the current sources with equivalent charges with a magnitude of $\vec{J}/\sigma$. To solve these equations, it is possible to use numerical partial differential equation solvers, or alternatively to simply add up the contributions of the different compartments: spherical somas and linear dendritic & axonal components. This calculation assumes a separation of the calculation of the trans-membrane potential and the extracellular potential, which is approximately correct[16-18]. The contribution of a spherical compartment is given by:

$$\Phi = \frac{I}{4\pi\sigma r} \tag{4}$$

And the contribution of a line positioned along the x axis (between 0 and *L*) is:

$$\Phi = \frac{I}{4\pi\sigma L}\ln\frac{x+\sqrt{x^2+y^2}}{(x-L)+\sqrt{(x-L)^2+y^2}} \tag{5}$$

The modeling studies offer a number of simple qualitative insights about extracellular recordings. First, the sign of the extracellular field does not directly correspond to the direction of local membrane currents. For example, in motor neurons a negative extracellular potential will be observed almost everywhere even when some parts of the cell membrane act as current sources and some as current sinks, with overall equality of sources and sinks. The concentrated sinks in the soma outweigh the low-density dendritic sources[74]. Second, within 10–20 μm from the axon hillock the extracellular field has a magnitude as large as a few millivolts[40]. Third, the temporal waveform of the extracellular field is fairly complex and varies significantly between different spatial locations around the neuron. For example, the extracellular waveform near the axon of a cortical pyramidal neuron contains a sequence of two negative spikes (observed experimentally in motoneurons[96]) probably as a result of superposition of the potentials due to the initial segment of the axon (the 'A' spike), and in the axon hillock (the 'B' spike[40]).

A number of experimental characterizations of the extracellular waveform were performed in the 1950's through the 1970's, mostly in an attempt to infer the mode of initiation and propagation of the action potential in different nerve cells (which can now be measured directly[95]). Several model CNS neuronal cells were studied, including spinal motor neurons, pyramidal cells in the neocortex and hippocampus and LGN neurons. The studies illustrated that extracellular spikes can often reverse their shape and polarity as a microelectrode is lowered into the CNS[79], and in a few cases provided a full mapping of the average spatiotemporal field[25,78].

Of particular interest from an experimental point of view is the question of the spread of the extracellular potential around a neuron when measured using metal microelectrodes, which directly translates to the ability to discern the signal above the noise level and to the number of units one expects to observe using a microelectrode. Several studies provided curves of the signal amplitude from isolated units while gradually inserting a microelectrode along a track using a micromanipulator[1,68]. The observed signal profile typically has peak amplitudes of a few hundred microvolts and a characteristic bell-shaped curve with a full width that depends on the particular neuron measured and on its distance from the track, but can provide a rough indication of the extracellular field extent. In the case of auditory cortical neurons in the cat such tracks appear to have a typical length of around 50 μm [1]. Using his dendritic motor-neuron model Rall[74] showed that the extracellular potential magnitude is expected to decay faster with distance from the soma than the 1/r decay characteristic of a Coulomb potential around a point source with an infinitely distant sink. Curves that characterize this decay were obtained from Rall's simulations[74] (but not for the more realistic neuron model[40]), and the radial current distribution was well fit by a decaying exponential. This leads to a radial potential distribution that is non-exponential, nevertheless, it can be viewed as approximately exponential over a restricted range. Measurements from a large number of closely spaced tetrodes in cat visual cortex, which were combined using the exponential approximation, yielded a decay constant of 28 μm. Using these empirical measurements it was approximated that neurons will be observable above noise level in a sphere of diameter ~130 μm.

Using a double-barreled glass microelectrode, Rosenthal[78] was able to estimate the lateral spread of the extracellular field of average pyramidal tract neurons in the cat, demonstrating that it roughly matched the relationship V(mV) ≈ 100/distance(μm). These measurements have implied a lateral spread that is over an order of magnitude larger than the spread measured by other methods, and it is possible that they are biased by 'giant' measurements where the electrodes are actually pushing against the neuron.

Recently, the potential spread was estimated directly for hippocampal area CA1 pyramidal neurons in the rat[37] by using coupled intracellular and extracellular recordings and measuring the distance between the electrode track and the actual neuron. These measurements suggest that cells within a 50 μm radius (twice that implied by Abeles[1]) from the extracellular microelectrode should be easily discernible. The study concludes that only a few percent of the expected number of units (estimated from the known

neuronal density) is actually seen in practice. This disturbing conclusion echoes similar observations made over three decades earlier by Robinson[77] using the theoretical predictions of Rall[74] regarding the spread of the extracellular potential. It may indeed imply that most neurons are largely silent during typical recording sessions[37], or have been silenced as a result of damage during electrode insertion. Alternatively, the source of the discrepancy may possibly be a systematic bias towards larger neurons affecting the spread estimates[37]. Finally, it may be the result of large anisotropies in the extracellular field brought about by glial cells that act as extracellular current barriers as originally suggested by Robinson[77], although a later study appeared to counter this claim[23]. This problem clearly indicates, however, that the spread and measurement of extracellular potential around CNS neurons is not yet well understood.

3. Multi-Unit Detection and Classification

In general, action potentials ("spikes") can be detected in the noisy extracellular signal ("spike detection"), and classified in terms of their source neurons ("spike sorting") in an attempt to reconstruct the underlying neural activity. Development of signal processing methods for spike detection and classification, which has been ongoing for at least four decades, has been fueled primarily by the dual goals of automating the reconstruction process while making it more reliable and accurate. At present neither full automation nor universal reliability have been achieved, and new methods continue to be developed. Reviews of both early and recent efforts can be found in the literature[55,84].

As a first approximation, the activity measured from each neuron during an action potential is a distinct, reproducible waveform, which is then contaminated by noise. Noise sources that affect spike shapes can be classified as additive and non-additive noise sources. Additive sources include Johnson noise in the electrode and electronics and background activity of distant neurons. The Johnson noise RMS magnitude is given by Nyquist's formula:

$$V_{RMS} = \sqrt{4k_B \cdot T \cdot R \cdot BW} \tag{6}$$

where k_B is Boltzmann's constant ($k_B = 1.38 \cdot 10^{-23}$ Joules/Kelvin), T is the temperature (in degrees Kelvin), R is the resistance (in Ohms) and BW is the recording bandwidth (in Hz). For an electrode with an impedance of 0.5 MΩ operating at 27^0C with a 7 kHz recording bandwidth, this implies an RMS noise level of ~7.6 μV, which may be elevated by additional thermal noise introduced by the amplifiers. Unless the electrode impedance is quite high, typical recordings in the CNS contain at least as much background activity as thermal noise[27]. Since the background noise is a sum of many, smaller spikes, it has a fairly similar spectral content to that of the primary waveforms we have to detect and sort[27], which poses a significant problem.

In addition to the additive sources of noise, several factors have a non-additive, distorting effect on the recorded waveforms. These include: waveform misalignment[54], the variation of the action potential shape as a function of recent firing history[27,73], and movement of the recording electrode[92].

The typical spike sorting process is schematically presented in Fig. 2 It starts with the detection of spikes in the raw digitized electrophysiological signal, typically by the use of a simple threshold detector. In those cases where recordings are performed by multiple electrodes acting as a sensor array, e.g., a tetrode or a multi-probe system[37], linear array denoising techniques[7,34] can be quite effective in improving the S/N ratio and the detection performance. The multiple views of the neural units, the noise sources, or both, may even provide enough information to make both the detection and classification steps trivial, e.g., by the use of blind source separation methods[10]. Such methods, however, appear to offer limited advantage in the single-channel case. In this case (independent views from different electrodes) pre-emphasis prior to detection may be possible based on quadratic or 'energy' operators[24,50].

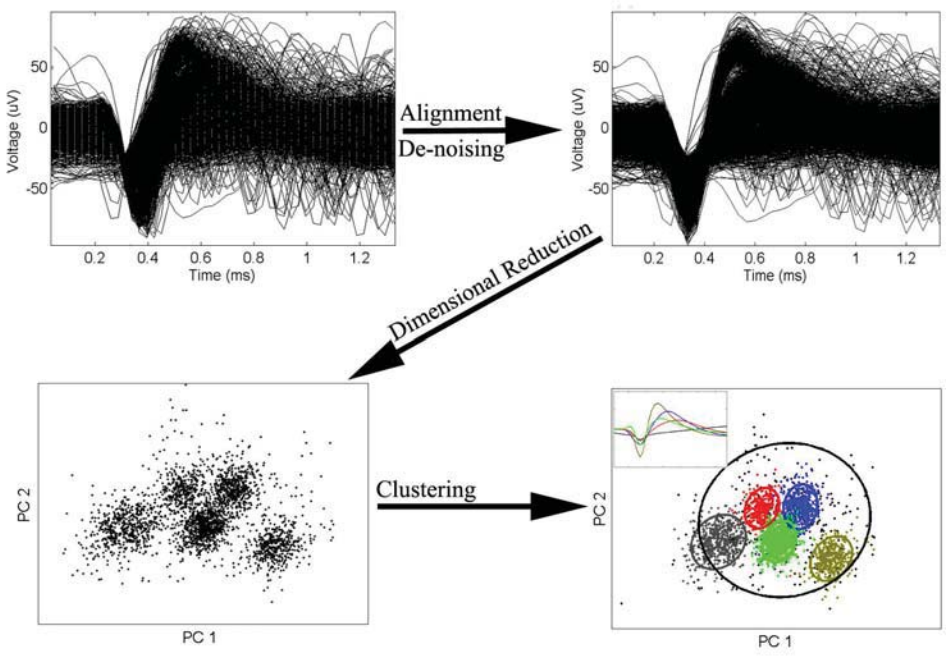

Fig. 2. Typical pre-processing and analysis steps used as part of spike sorting.

Following detection, an effort is typically made to remove some of the variation from the collected waveforms. Alignment procedures have been developed to compensate for the distortions resulting from waveform misalignment, by aligning the

waveforms to their center of mass[27] or peaks[80]. By using waveform interpolation schemes, these procedures can achieve a temporal accuracy much better than the sampling frequency. Alternatively, waveform alignment can be preformed as part of the clustering process by aligning to the evolving templates during each iteration[54]. Additional de-noising can be achieved by using a Wiener-type filter when the properties of the signal and noise are fairly well characterized[27].

In most spike sorting programs the waveform dimensionality is reduced by moving from the high-dimensional sampled waveforms (typically 20-60 dimensions) to a projection on a small subset of discriminating features (typically 2-6 dimensions). Dimensional reduction was originally introduced as an aid to visualization and manual clustering; however, it also provides a great reduction in computational complexity in automatic classification procedures, and may actually improve the performance of certain algorithms. Since it is important to preserve as much of the discriminating information as possible for the classification stage, dimensional reduction relies on the observation that in the typical waveform data such information is highly concentrated in a relatively low-dimensional subspace[27]. Many methods for selecting a set of discriminating features have been developed[84]. Particularly popular is the method of principal components analysis[2] (PCA) that creates a set of orthogonal features that corresponds to directions of maximal variance in the data. Recent studies introduced a noise-robust version of PCA[80], and wavelet-packet based dimensional reduction[42]. A new method based on Projection-Pursuit provides discriminating features with a superior discriminating power to those obtained using PCA[51].

Deriving the classification templates from the collection of waveforms or waveform features is a clustering (or *unsupervised* classification) problem except in those cases where individual neurons can be independently driven[64], where it is a *supervised* classification task[43]. This, however, is seldom the case in CNS recordings. Most existing software packages still employ a human user that defines the class boundaries, typically assisting the user by providing multiple views of the data projected onto the reduced feature set. However, a number of methods now exist for automatic spike clustering, using various iterative learning procedures. While a few automatic clustering methods were developed specifically for clustering neural spikes[26,92] most of the published methods are adaptations of general methods for unsupervised pattern recognition[43]. These include algorithms such as k-means[81], fuzzy c-means[104], artificial neural-network based clustering schemes[29,50,70] and finite mixture decomposition[54,55,80,89].

Finite mixture decomposition has the advantage of being particularly well suited to clustering when the individual clusters are elongated (that is, non-spherical), with different clusters having either the same or different shapes. It provides an explicit yet flexible statistical framework that can also address the issue of automatically selecting the number of clusters[28,55,63]. In mixture modeling we assume that each of the N points $\mathbf{x}_i$ (in general, $\mathbf{x}_i$ is a vector) originates from one of g components. In spike sorting, $\mathbf{x}_i$ represents a sampled spike waveform or a vector of features, and the different components correspond to different units (some components may be non-units that collect 'garbage'

waveforms). Assuming that each unit accounts for a proportion π_j of the total spikes, and that the distribution of spikes from unit j has parameters θ_j, the likelihood of the data (the probability of obtaining the given data set from this model) is[55,63]:

$$p(\mathbf{x}_1 ... \mathbf{x}_N) = \prod_{i=1}^{N} p(\mathbf{x}_i) = \prod_{i=1}^{N} \sum_{j=1}^{g} \pi_j p(\mathbf{x}_i \mid \theta_j) \tag{7}$$

The best-fitting model parameters $\left\{\pi_{1...g}, \theta_{1...g}\right\}$ are determined by maximizing the model likelihood, or its logarithm (the 'log-likelihood', *L*), which always requires an iterative algorithm. The most popular log-likelihood maximization algorithms used for this task are the family of Expectation-Maximization (EM) algorithms[63].

What is $p(\mathbf{x}_i \mid \theta_j)$, the distribution of spikes from unit j? The first mixture model of spike waveforms[54] used an isotropic, spherical Gaussian model of neural waveform statistics; however, in later work the shortcomings of spherical clusters as models of neural variability were demonstrated[27] and current implementations use an assortment of elliptical multivariate gaussians as a model of both the neural units and the collection of 'garbage' waveforms[55]:

$$p(\mathbf{x}_i \mid \theta_j) = p(\mathbf{x}_i \mid \boldsymbol{\mu}_j, \boldsymbol{\Sigma}_j) = \frac{1}{(2\pi)^{p/2} \left|\boldsymbol{\Sigma}_j\right|^{1/2}} \exp(-\delta(\mathbf{x}_i, \boldsymbol{\mu}_j; \boldsymbol{\Sigma}_j)/2) \tag{8}$$

Where $\delta(\mathbf{x}_i, \boldsymbol{\mu}_j; \boldsymbol{\Sigma}_j) = \left(\mathbf{x}_i - \boldsymbol{\mu}_j\right)^T \boldsymbol{\Sigma}_j^{-1} \left(\mathbf{x}_i - \boldsymbol{\mu}_j\right)$ is the squared Mahalanobis distance between the *p*-dimensional data point $\mathbf{x}_i$ and the template $\boldsymbol{\mu}_j$ with covariance $\boldsymbol{\Sigma}_j$ (when $\boldsymbol{\Sigma}_j$ is diagonal, this is the familiar Euclidian distance). The multivariate Gaussian is itself an inadequate model of the waveform distribution[35,89] which tends to have significant 'tails', and a recent study[90] introduced a new model using multivariate t-distributions, which are similar to Gaussians but better describe the observed noise statistics:

$$p(\mathbf{x}_i \mid \boldsymbol{\mu}_j, \boldsymbol{\Sigma}_j, \nu) = \frac{\Gamma\left(\frac{\nu + p}{2}\right)}{\Gamma\left(\frac{\nu}{2}\right)(\pi\nu)^{p/2} \left|\boldsymbol{\Sigma}_j\right|^{1/2}} \times \frac{1}{\left[1 + \frac{\delta(\mathbf{x}_i, \boldsymbol{\mu}_j; \boldsymbol{\Sigma}_j)}{\nu}\right]^{(\nu+p)/2}} \tag{9}$$

Where ν is the 'degrees of freedom' (DOF) parameter, which tunes the tails of the distribution, and Γ is the Gamma function.

Unlike the model parameters determination, the number of components cannot be found by maximizing the likelihood, as it affects the statistical model order and complexity. Adding more components will always allow for a better likelihood, and a variety of information based penalized-likelihood functions have been developed that compensate for this tendency. These include Akaike's information criterion[101] (AIC), the Bayesian information criterion[87] (BIC), and the Minimum-message length[28] (MML) criterion. Comparison of the different number of components can be carried out by repeatedly fitting the mixture models of different orders, and then comparing the best results, a procedure which is computationally quite demanding. A more economical approach is to use optimization procedures that quickly move across model sizes by either splitting components[80] or eliminating them. Component elimination can be performed either competitively[28,89] as part of the clustering process or subsequently by finding the modes of the estimated mixture model[51]. Mixture model based approaches are quite flexible and allow the incorporation of domain-specific information. A recently developed algorithm accounted for refractory periods and waveform changes during bursts[80].

An additional challenge in spike sorting is decomposing overlapping waveforms, and is best addressed after the characteristic waveforms (or templates) of the different neurons are computed. Possible solutions to this complex problem include exhaustive comparison of each waveform to all possible overlapping waveforms[3], a more efficient version of this exhaustive search[54], and an artificial neural network based approach[14]. All of these methods are computationally expensive either in terms of an initial training period, or in terms of the comparisons that need to be executed. A "greedy" algorithm is presented in[80]; however it will work only when the waveforms have minimal overlap or when multiple channels are available.

The different algorithms developed for multiunit classification possess widely different performance characteristics. A recent experimental study[35] acquired a unique data set, where the sources of the extracellularly recorded spikes were validated using simultaneous intracellular recordings. This and similar datasets can now serve as objective benchmarks for the performance of spike classification algorithms.

4. Local-field Potential and Far-field Recordings

Receptive field properties of local-field potentials from microelectrodes are found to be largely similar to those of spiking neurons. It is commonly accepted that the low-frequency field potential recordings reflect synaptic inputs while the spiking process is a reflection of the output transformation at the recording site[56,57]. Recent studies have indicated, however, that in certain cases the field potentials are also related to slow processes related to firing, such as after-hyperpolarization[11]. In the near-field (~100–300 μm), recordings are dominated by the source currents and simple volume-conduction effects. These effects can usually be modeled as quasi-static sources located in semi-

infinite or bounded (usually spherical) volume conductors and the resulting electric potentials and magnetic fields are governed by the equations:

$$\Phi(\mathbf{r}) = -\frac{1}{4\pi\sigma}\int_V \frac{\nabla\times\mathbf{J}(\mathbf{r})}{|\mathbf{r}-\mathbf{r}'|}d^3r \tag{10}$$

$$\mathbf{B}(\mathbf{r}) = -\frac{\mu}{4\pi}\int_V \mathbf{J}\times\nabla\frac{1}{|\mathbf{r}-\mathbf{r}'|}d^3r \tag{11}$$

where $\mathbf{J}$ is the distribution of current sources and sinks. In most cases, the source currents can be modeled as equivalent current dipoles. In some cases, multipolar expansion terms need to be included for source currents[45,97].

Local-field potential measurements obtained from different laminae are commonly used to identify laminar sources and sinks of synaptic currents using a technique known as current-source density imaging[66]. The theory underlying current-source density is that in a one-dimensional case the potential is described by the following equation:

$$i_v(x) \propto \frac{\partial^2 V}{\partial x^2} \tag{12}$$

where $i_v(x)$ reflects the position of a sources and sinks. Therefore, a simple method to reconstruct source-sink distributions is to obtain an approximation to the second-spatial derivative of the potentials at different laminae. Similarly, in far-field recordings, Laplacian operations are performed on the potentials (three-dimensional second derivatives) to reconstruct the location of sources and sinks[69,102].

Fields generated by single-neurons are much too small to be detected beyond the vicinity of a few hundred micrometers. A fortuitous anatomical feature of cortex where many cells are aligned systematically to the cortical surface allows for fields of synchronous neurons to superpose (Fig. 3). This superposition renders signals that can be measured several millimeters away. The closest "far-field" measurements are EcoG signals from the pial or sub-dural surfaces which demonstrate similar frequency characteristics to local-field potentials obtained from depth microelectrodes[19-21]. However, EcoG electrodes are much larger in size and typically measure activity from several millimeters. The most-common far-field recordings are EEG/MEG signals recorded on the surface of the scalp. Single EEG/MEG measurements are usually sensitive to volumes as much as 100 cm^2 on cortex. Combining several measurements leads to maximizing spatial resolution on the order of 1 cm^2. Therefore, these measurements typically span the activity of 10^7–10^9 neurons. Crossing the barrier of the skull violates the assumption of a homogenous and semi-infinite volume conductor and

boundary conditions play an important role. The skull is a poor conductor that is anisotropic. These factors greatly attenuate and spatially distort the electric potentials recorded at the scalp. Equations for the potential on the scalp have to include the complex boundaries between the cortex, pia, skull and scalp. In contrast, magnetic fields measured by MEG are not attenuated by the skull and can be more easily reconstructed.

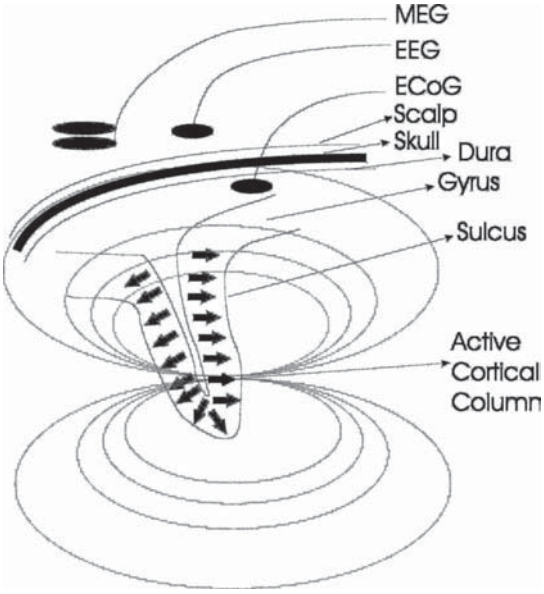

Fig. 3. Schematic illustration of near- and far-field recording methods. Cortical columns are often approximated by dipole current sources shown as arrows. An active current dipole is highlighted in gray and the current flow patterns from this source are shown as dotted lines. Electrocorticogram (ECoG) recordings are measured directly on the cortical surface using sub-dural electrodes, while Electroencephalographic (EEG) signals are measured noninvasively from the scalp. Magnetoencephalography (MEG) recordings of weak magnetic fields (femtoTesla) are measured using superconducting quantum interference device magnetometers (SQUIDs).

5. Representation of Time-varying Information in Spike Trains

Neurons throughout the CNS represent, communicate, and process information that is present in the form of time series of all-or-none action potentials. The activity of individual neurons and/or neural populations represents or 'encodes' dynamically varying features of sensory stimuli from the external world as well as internal representations that are related to cognitive processes or upcoming motor actions. Since the nervous system has a distributed architecture that is both hierarchical and recurrent such representations have to be read or 'decoded' by other parts of the CNS. Thus, encoding and decoding are two essential components in an understanding of information representation in the CNS.

The mathematical framework that is relevant for describing information-carrying series of spikes is the theory of random point processes[93]. Much of the modern theory of point processes was developed by engineers interested in applications that included optical communication (at the limit of low photon counts), nuclear imaging (PET and SPECT) and neural codes. Within this framework encoding can be viewed as a *generative model* that relates the point process 'output' to the variables of interest as well as various noise sources, whereas decoding is viewed as the problem of estimating the variable of interest from the activity of one or more point processes. The time series of spikes can be described completely (and therefore equivalently) in terms of the times of spike occurrence, the sequence of inter-spike intervals (ISIs), or a counting process (also termed a jump process) that increases by 1 at every spike and is therefore the integral of the point process. In contrast, the total number of spikes in a time window, or spike *count*, is not an equivalent description, since it loses information about the timing of spikes. It is nevertheless a useful measure, often used in the analysis of neural data.

In a random point process each time is associated a non-negative intensity $\lambda(t)$ which is the probability of obtaining a point at that time. The intensity is an instantaneous firing rate and, in general, depends on experimental time-varying conditions and on the timing of previous spikes (we will use $\lambda(t \mid H_t)$ to denote the dependence on History up to time t). The homogenous Poisson process is the simplest point process, having a constant intensity $\lambda(t) = c$. If the intensity depends only on time, an inhomogeneous Poisson process results $\lambda(t) = c(t)$. In both of these cases the distribution of spike counts in a finite time window is a Poisson distribution with a mean and variance that are equal to the integral of the intensity:

$$\Pr(N = k) = \frac{e^{-\int_{t_0}^{T} \lambda(t)\,dt} \left(\int_{t_0}^{T} \lambda(t)\,dt \right)^k}{k!} \tag{13}$$

A large number of point process models exist that are more general than the Poisson process[93]. Typical models rely on conditioning the intensity on the recent firing history ('self exciting' point processes), or on making the intensity λ(t) itself into a random process ('doubly stochastic Poisson' or 'Cox processes'). We will review below some of the models used in the context of encoding models of CNS neurons.

6. Stimulus Encoding in CNS Spike Trains

A small number of cortical systems have emerged in recent years as model experimental systems for the study of neural information encoding. These systems include place cells

in the rat's hippocampus[4,9,44,103], the visual-motion sensitive neurons in area MT (Medio-Temporal) of the primate's brain[91], and hand-motion sensitive neurons in area MI (primary motor cortex) of primates[31,67,89]. The basic encoding relationship that most models are concerned with is the dependence of firing rate of individual neurons on the variables of interest. This dependence is typically modeled as a simple static nonlinear relationship[9,31,67].

$$\lambda(t) = \begin{cases} MI\ \ direction\ \ encoding\ : a_0 + a_1 \cos(\theta(t) - \theta_{pref}) \\ MI\ \ velocity\ \ encoding\ : a_0 + a_1 V_x(t) + a_2 V_y(t) + a_3 \left|\vec{V}(t)\right| \\ Place\ \ encoding\ : a_0 \exp\left(- \left(x(t) - x_{pref}\right)^2 / \sigma_x^{\,2} - \left(y(t) - y_{pref}\right)^2 / \sigma_y^{\,2} \right) \end{cases} \tag{14}$$

A more sophisticated model for firing rate is one where a general linear filtering operation takes place before the static nonlinearity, leading to a linear-nonlinear (LN) system model[15]. Such models have been used to describe encoding in visual neurons[13], and in MI neurons during complex behavior[89]. Models where an additional linear kernel is added after the nonlinearity are known as LNL models. More general approximations of functional dependence can be provided by Volterra series expansions[59] or other universal approximations. The use of these general representations is typically dependent on the use of specific stimulus types and is often biologically vague. Several studies of visual cortical responses[12,36,91] have suggested a simple model for feedback interaction of neurons in a local neighborhood that implements divisive normalization of the firing rate of individual neurons. This operation is suggested to follow after an LN type of feed-forward dependence on the stimulus. A method for identifying such gain-controlled LN models from data has recently been developed[86].

What noise models are used to describe the variability of the neural spike trains? As we have mentioned above different representations of the spike trains can be used, usually in conjunction with noise models that are easiest to work with in this representation. The most basic noise model is the Poisson model, which can be used with all representations: a Poisson process arises when the probabilities of spiking at different times are independent of each other (no memory), it has a spike count distribution given by Eq. (13), and is associated with an exponential distribution for the (inter-spike interval) ISI time intervals. While a large number of analytical discrete distributions exist in the literature[46] and can be used to fit the count distributions, it appears that most non-Poisson modeling of neural spike trains is in terms of self-exciting models and ISI distributions.

A couple of studies[33,61] that looked at cortical spike counts over extended time windows used truncated Gaussians to fit the data, and a recent study[89] introduced a new

discrete probability distribution termed the Normalized-Gaussian distribution specifically for the purpose of describing the count statistics of MI cortical neurons. Non-exponential ISI distributions can be based on any non-negative continuous univariate distribution[47]. Popular choices include the Gamma distribution (which has the exponential as a special case), the Lognormal distribution, and the Inverse-Gaussian distribution[4,98]. These models have an extra parameter that facilitates fitting more general ISI distributions. While traditionally non-Poisson ISI models were used as renewal models, that is, in the context of a constant firing rate, recently they are being used in non-stationary (or inhomogeneous) models using the method of time-rescaling[4,8,72]. This method relies on transforming the spike times to a new time scale defined by the integral of the intensity function obtained from the model:

$$\Lambda(\tau_k) = \int_0^{\tau_k} \lambda(\tau \mid H_\tau)\, d\tau \tag{15}$$

If the intensity model is correct, the spike train is transformed into a Poisson process with constant rate 1, an assertion that can be tested using simple statistical tools.

Beginning with studies of spike trains from sensory afferents, a few studies[5,30,49,58] have utilized a different variability model where the intensity is a product of two terms: one that depends on the experimental time(λ_1), and one that represents a recovery after each spike(λ_2).

$$\lambda(t \mid H_\tau) = \lambda_1(t) \cdot \lambda_2(t - \tau_k) \tag{16}$$

This product model can be viewed as a special case of Inhomogeneous Markov-Interval models[49]. To date, none of the 'neural noise' models we've listed has been used as a multivariate model, except in the context of spike counts where a multivariate gaussian was used as an approximation[61]. Nevertheless, much interest does exist currently regarding the multivariate firing properties of neurons, particularly as they manifest in synchronous firing patterns.

Methods for decoding the activity of neural populations can be broken down according to whether they are based on a statistical model of the firing, whether they are linear or nonlinear, and according to whether they are dynamical or static. Perhaps the simplest and most popular decoding method is the Population Vector method[32], where each neuron's spike count multiplies a 'preferred direction' vector associated with this neuron. The sum of all such vectors represents the decoding result, e.g., the direction of motion of the monkey's arm in the study by Georgopoulos[32].

The population vector is a linear decoding technique that is not model-based. When one considers the noise statistics of the recorded neurons, it is easy to find optimal linear estimators[82] and optimal nonlinear estimators[61,71,83,88], which significantly differ from the population vector. The optimal nonlinear estimators are obtained using statistical

optimization criteria such as the Maximum Likelihood Estimate (MLE). The Population Vector is also not a dynamical estimator — estimation in each time bin is considered separately. In applications where the Population Vector was used to estimate time varying quantities, a separate filter was used to smooth the independent estimates in the different time bins[85]. Recently, a number of studies used optimal linear filters for dynamical decoding in single neurons and neural populations[6,76,94,99,100]. These filters can be calculated using standard linear regression techniques, and the neural spike trains are simply convolved with them to obtain the dynamical estimate. In contrast, optimal nonlinear estimation relies on a nonlinear filter that is specifically tailored to the statistical model of the neuron firing and the dynamics of the variable of interest. It requires a recursive update not only of the estimate, but also of a full conditional distribution across the possible values of the estimate. Examples using recursive nonlinear filters have also been developed by a few recent studies in an attempt to decode the activity of Hippocampal place cells[9,103] as well as MI neurons[89].

While nonlinear optimal dynamical estimation is much more complex than linear ones, it enjoys renewed interest in the engineering and applied math community, particularly due to the recent development of Sequential Monte Carlo filters[22]. What method of decoding is likely to be performed by real networks operating in the brain? From a theoretical point of view it is possible to see networks of neurons or even single neurons[65] performing arbitrarily complex nonlinear computations, which leaves us currently with no handle on this question.

7. Conclusions

Recent years have seen a quickly growing interest in neural interfaces with the CNS. Novel electrode array designs, functional imaging methods (like optical imaging, fMRI and MEG) and microscopy techniques have also been developed. Many of the questions we've surveyed above remain at least partially open, and these new tools or their combination with traditional methods may help shed new light. The sustained exponential growth in computing power has enabled the implementation of highly sophisticated models and data analysis methods, in some cases in real time.

As we've noted, no current spike sorting method has reached the desirable levels of automation and reliability, in spite of the use of some of the best currently available detection and pattern recognition methods. Not all applications require high sorting reliability; however, such a characteristic is desired for universal applicability. While much can still be gained from improvements in signal processing methods, the current trend in electrode array design appears to lead towards dense 3-D arrays of low impedance electrodes. In this configuration, spike sorting will be performed using array signal processing methods, potentially using a 'blind' method like independent component analysis. A better understanding of the extent of extracellular potential spread is desirable for the design of these arrays. Likewise, the increasing number of units

recorded using electrode arrays (recently, 800 units were recorded in a single monkey[39]) begs the development of better computational tools for analyzing this data, primarily under dynamical, non-stationary conditions.

References

1 Abeles, M. *Local Cortical Circuits*. Berlin: Springer Verlag, 1982.

2 Abeles, M., and M. H. Goldstein. Multispike train analysis. *Proc. IEEE* 65:762-773, 1977.

3 Atiya, A. F. Recognition of multiunit neural signals. *IEEE Trans Biomed Eng* 39:723-9, 1992.

4 Barbieri, R., M. C. Quirk, L. M. Frank, M. A. Wilson, and E. N. Brown. Construction and analysis of non-Poisson stimulus-response models of neural spiking activity. *J Neurosci Methods* 105:25-37, 2001.

5 Berry, M. J., 2nd, and M. Meister. Refractoriness and neural precision. *J Neurosci* 18:2200-11, 1998.

6 Bialek, W., F. Rieke, R. R. de Ruyter van Steveninck, and D. Warland. Reading a neural code. *Science* 252:1854-7, 1991.

7 Bierer, S. M., and D. J. Anderson. Multi-channel Spike Detection and Sorting using an Array Processing Technique. *Neurocomputing* 26-27:947-956, 1999.

8 Brown, E. N., R. Barbieri, V. Ventura, R. Kass, and L. M. Frank. The time-rescaling theorem and its application to neural spike train data analysis. *Neural Comput* 14:325-346, 2001.

9 Brown, E. N., L. M. Frank, D. Tang, M. C. Quirk, and M. A. Wilson. A statistical paradigm for neural spike train decoding applied to position prediction from ensemble firing patterns of rat hippocampal place cells. *J Neurosci* 18:7411-25, 1998.

10 Brown, G. D., S. Yamada, and T. J. Sejnowski. Independent component analysis at the neural cocktail party. *Trends Neurosci* 24:54-63, 2001.

11 Buzsaki, G., and R. D. Traub. Generation of EEG. In: *Epilepsy: a comprehensive textbook*, edited by J. a. T. A. P. J. Engel Lippincott-Raven Press, 1996.

12 Carandini, M., D. J. Heeger, and J. A. Movshon. Linearity and normalization in simple cells of the macaque primary visual cortex. *J Neurosci* 17:8621-44., 1997.

13 Chander, D., and E. J. Chichilnisky. Adaptation to temporal contrast in primate and salamander retina. *J Neurosci* 21:9904-16., 2001.

14 Chandra, R., and L. M. Optican. Detection, classification, and superposition resolution of action potentials in multiunit single-channel recordings by an on-line real-time neural network. *IEEE Trans Biomed Eng* 44:403-12, 1997.

15 Chichilnisky, E. A simple white noise analyses of neuronal light responses. *Network: Comput. Neural Sys.* 12:199-213, 2001.

[16] Clark, J., and R. Plonsey. A mathematical evaluation of the core conductor model. *Biophys J* 6:95-112, 1966.

[17] Clark, J., and R. Plonsey. The extracellular potential field of the single active nerve fiber in a volume conductor. *Biophys J* 8:842-64, 1968.

[18] Clark, J. W., and R. Plonsey. A mathematical study of nerve fiber interaction. *Biophys J* 10:937-57, 1970.

[19] Crone, N. E. Functional mapping with ECoG spectral analysis. *Adv Neurol* 84:343-51, 2000.

[20] Crone, N. E., D. Boatman, B. Gordon, and L. Hao. Induced electrocorticographic gamma activity during auditory perception. Brazier Award-winning article, 2001. *Clin Neurophysiol* 112:565-82, 2001.

[21] Crone, N. E., D. L. Miglioretti, B. Gordon, and R. P. Lesser. Functional mapping of human sensorimotor cortex with electrocorticographic spectral analysis. II. Event-related synchronization in the gamma band. *Brain* 121 (Pt 12):2301-15, 1998.

[22] Doucet, A., N. d. Freitas, and N. Gordon. Sequential Monte Carlo Methods in Practice. Springer Verlag, 2001.

[23] Drake, K. L., K. D. Wise, J. Farraye, D. J. Anderson, and S. L. BeMent. Performance of planar multisite microprobes in recording extracellular single-unit intracortical activity. *IEEE Trans Biomed Eng* 35:719-32., 1988.

[24] Fang, J., and L. E. Atlas. Quadratic detectors for energy estimation. *IEEE Transactions on Signal Processing* 43:2582-2594, 1995.

[25] Fatt, P. Electric potentials occuring around a neurone during its antidromic activation. *J Neurophysiol* 20:27-60, 1957.

[26] Fee, M. S., P. P. Mitra, and D. Kleinfeld. Automatic sorting of multiple unit neuronal signals in the presence of anisotropic and non-Gaussian variability. *J Neurosci Methods* 69:175-88, 1996.

[27] Fee, M. S., P. P. Mitra, and D. Kleinfeld. Variability of extracellular spike waveforms of cortical neurons. *J Neurophysiol* 76:3823-33, 1996.

[28] Figueiredo, M., and A. Jain. Unsupervised learning of finite mixture models. *IEEE Trans on PAMI* 24:381-396, 2002.

[29] Garcia, P., C. P. Suarez, J. Rodriguez, and M. Rodriguez. Unsupervised classification of neural spikes with a hybrid multilayer artificial neural network. *J Neurosci Methods* 82:59-73, 1998.

[30] Gaumond, R. P., C. E. Molnar, and D. O. Kim. Stimulus and recovery dependence of cat cochlear nerve fiber spike discharge probability. *J Neurophysiol* 48:856-73, 1982.

[31] Georgopoulos, A. P., J. F. Kalaska, R. Caminiti, and J. T. Massey. On the relations between the direction of two-dimensional arm movements and cell discharge in primate motor cortex. *J Neurosci* 2:1527-37, 1982.

[32] Georgopoulos, A. P., A. B. Schwartz, and R. E. Kettner. Neuronal population coding of movement direction. *Science* 233:1416-9, 1986.

[33] Gershon, E. D., M. C. Wiener, P. E. Latham, and B. J. Richmond. Coding strategies in monkey V1 and inferior temporal cortices. *J Neurophysiol* 79:1135-44, 1998.

[34] Gozani, S. N., and J. P. Miller. Optimal discrimination and classification of neuronal action potential waveforms from multiunit, multichannel recordings using software-based linear filters. *IEEE Trans Biomed Eng* 41:358-72, 1994.

[35] Harris, K. D., D. A. Henze, J. Csicsvari, H. Hirase, and G. Buzsaki. Accuracy of tetrode spike separation as determined by simultaneous intracellular and extracellular measurements. *J Neurophysiol* 84:401-14, 2000.

[36] Heeger, D. J. Normalization of cell responses in cat striate cortex. *Vis Neurosci* 9:181-97., 1992.

[37] Henze, D. A., Z. Borhegyi, J. Csicsvari, A. Mamiya, K. D. Harris, and G. Buzsaki. Intracellular features predicted by extracellular recordings in the hippocampus in vivo. *J Neurophysiol* 84:390-400, 2000.

[38] Hines, M. L., and N. T. Carnevale. The NEURON simulation environment. *Neural Comput* 9:1179-209., 1997.

[39] Hoffman, K. L., and B. L. McNaughton. Coordinated reactivation of distributed memory traces in primate neocortex. *Science* 297:2070-3., 2002.

[40] Holt, G. R., and C. Koch. Electrical interactions via the extracellular potential near cell bodies. *J Comput Neurosci* 6:169-84., 1999.

[41] Hubbard, J. I., R. Llinas, and D. M. J. Quastel. Electrophysiological analysis of synaptic transmission. London: Edward Arnold, 1969, pp. 265-293.

[42] Hulata, E., R. Segev, and E. Ben-Jacob. A method for spike sorting and detection based on wavelet packets and Shannon's mutual information. *J Neurosci Methods* 117:1-12, 2002.

[43] Jain, A. K., R. P. W. Duin, and J. Mao. Statistical Pattern Recognition: A Review. *IEEE Trans. Pattern Anal. Mach. Intell.* 22:4-37, 2000.

[44] Jensen, O., and J. E. Lisman. Position reconstruction from an ensemble of hippocampal place cells: contribution of theta phase coding. *J Neurophysiol* 83:2602-9, 2000.

[45] Jerbi, K., J. C. Mosher, S. Baillet, and R. M. Leahy. On MEG forward modelling using multipolar expansions. *Phys Med Biol* 47:523-55, 2002.

[46] Johnson, N. L., and S. Kotz. *Discrete distributions*. Boston: Houghton Mifflin, 1969.

[47] Johnson, N. L., S. Kotz, and B. N. *Continuous Univariate Distributions*. New York: John Wiley & Sons, 1994.

[48] Johnston, D., and M.-S. W. Wu. *Foundations of Cellular Neurophysiology*. Cambridge, Mass.: MIT Press, 1994.

[49] Kass, R. E., and V. Ventura. A spike-train probability model. *Neural Comput* 13:1713-20., 2001.

[50] Kim, K. H., and S. J. Kim. Neural spike sorting under nearly 0-dB signal-to-noise ratio using nonlinear energy operator and artificial neural-network classifier. *IEEE Trans Biomed Eng* 47:1406-11, 2000.

[51] Kim, K. H., and S. J. Kim. Method for unsupervised classification of multiunit neural signal recording under low signal-to-noise ratio. *IEEE Trans Biomed Eng*:, In press.

[52] Koch, C. *Biophysics of computation: information processing in single neurons*. New York: Oxford University Press, 1999.

[53] Lemon, R. *Methods for neuronal recording in conscious animals*. IBRO handbook series: Methods in the neurosciences, 4. New York: Wiley, 1984.

[54] Lewicki, M. S. Bayesian modeling and classification of neural signals. *Neural Computation* 6:1005-1030, 1994.

[55] Lewicki, M. S. A review of methods for spike sorting: the detection and classification of neural action potentials. *Network* 9:R53-78, 1998.

[56] Logothetis, N. K. The neural basis of the blood-oxygen-level-dependent functional magnetic resonance imaging signal. *Philos Trans R Soc Lond B Biol Sci* 357:1003-37., 2002.

[57] Lorente de No, R. *A study of nerve physiology*. Studies from the Rockefeller Institute for Medical Research, 131-132, 1947.

[58] Mark, K. E., and M. I. Miller. Bayesian model selection and minimum description length estimation of auditory-nerve discharge rates. *J Acoust Soc Am* 91:989-1002, 1992.

[59] Marmarelis, V. Z. Modeling methodology for nonlinear physiological systems. *Ann Biomed Eng* 25:239-51, 1997.

[60] Matthews, R. T., and W. L. Lee. A comparison of extracellular and intracellular recordings from medial septum/diagonal band neurons in vitro. *Neuroscience* 42:451-62., 1991.

[61] Maynard, E. M., N. G. Hatsopoulos, C. L. Ojakangas, B. D. Acuna, J. N. Sanes, R. A. Normann, and J. P. Donoghue. Neuronal interactions improve cortical population coding of movement direction. *J Neurosci* 19:8083-93, 1999.

[62] McCormick, D. A., B. W. Connors, J. W. Lighthall, and D. A. Prince. Comparative electrophysiology of pyramidal and sparsely spiny stellate neurons of the neocortex. *J Neurophysiol* 54:782-806., 1985.

[63] McLachlan, G. J., and D. Peel. *Finite Mixture Models*. New York: Wiley, 2000.

[64] McNaughton, T. G., and K. W. Horch. Action potential classification with dual channel intrafascicular electrodes. *IEEE Trans Biomed Eng* 41:609-16, 1994.

[65] Mel, B. W. Information processing in dendritic trees. *Neural Comput* 6:1031-1085, 1994.

[66] Mitzdorf, U. Current source-density method and application in cat cerebral cortex: investigation of evoked potentials and EEG phenomena. *Physiol Rev* 65:37-100, 1985.

[67] Moran, D. W., and A. B. Schwartz. Motor cortical representation of speed and direction during reaching. *J Neurophysiol* 82:2676-92, 1999.

[68] Mountcastle, V. B., P. W. Davies, and A. L. Berman. Response properties of neurons of cat's somatic sensory cortex to peripheral stimuli. *J Neurophysiol* 20:374-407, 1957.

[69] Nunez, P. L., and A. F. Westdorp. The surface Laplacian, high resolution EEG and controversies. *Brain Topogr* 6:221-6, 1994.

[70] Ohberg, F., H. Johansson, M. Bergenheim, J. Pedersen, and M. Djupsjobacka. A neural network approach to real-time spike discrimination during simultaneous recording from several multi-unit nerve filaments. *J Neurosci Methods* 64:181-7, 1996.

[71] Oram, M. W., P. Foldiak, D. I. Perrett, and F. Sengpiel. The 'Ideal Homunculus': decoding neural population signals. *Trends Neurosci* 21:259-65, 1998.

[72] Papangelou, F. Integrability of Expected Increments of Point Processes and Related Random Changes of Scale. *Transactions of the American Mathematical Society* 165:483-506, 1972.

[73] Quirk, M. C., and M. A. Wilson. Interaction between spike waveform classification and temporal sequence detection. *J Neurosci Methods* 94:41-52, 1999.

[74] Rall, W. Electrophysiology of a dendritic neuron model. *Biophys J* 2:145-167, 1962.

[75] Rao, S. G., G. V. Williams, and P. S. Goldman-Rakic. Isodirectional tuning of adjacent interneurons and pyramidal cells during working memory: evidence for microcolumnar organization in PFC. *J Neurophysiol* 81:1903-16., 1999.

[76] Rieke, F., D. Warland, R. R. de Ruyter van Stevenink, and W. Bialek. *Spikes; Exploring The Neural Code*: MIT Press, 1996.

[77] Robinson, D. A. The electrical properties of metal microelectrodes. *Proc. IEEE* 56:1065-1071, 1968.

[78] Rosenthal, F. Extracellular potential fields of single PT-neurons. *Brain Res* 36:251-63., 1972.

[79] Rosenthal, F., J. W. Woodbury, and H. D. Patton. Dipole characteristics of pyramidal cell activity in cat postcruciate cortex. *J Neurophysiol* 29:612-25., 1966.

[80] Sahani, M. *Latent Variable Models for Neural Data Analysis*. Ph.D. Dissertation. Computation and Neural Systems. California Institute of Technology, 1999.

[81] Salganicoff, M., M. Sarna, L. Sax, and G. L. Gerstein. Unsupervised waveform classification for multi-neuron recordings: a real-time, software-based system I Algorithms and implementation. *J Neurosci Methods* 25:181-7, 1988.

[82] Salinas, E., and L. F. Abbott. Vector reconstruction from firing rates. *J Comput Neurosci* 1:89-107, 1994.

[83] Sanger, T. D. Probability density estimation for the interpretation of neural population codes. *J Neurophysiol* 76:2790-3, 1996.

[84] Schmidt, E. M. Computer separation of multi-unit neuroelectric data: a review. *J Neurosci Methods* 12:95-111, 1984.

[85] Schwartz, A. B. Direct cortical representation of drawing. *Science* 265:540-2, 1994.

[86] Schwartz, O., E. J. Chichilnisky, and E. P. Simoncelli. Characterizing neural gain control using spike-triggered covariance. In: *Advances in Neural Information Processing Systems*, edited by T. G. Dietterich, S. Becker and Z. Ghahramani. Cambridge: MIT Press, 2002, pp. 269-276.

[87] Schwarz, G. Estimating the dimesnions of a model. *Annals of Statistics* 6:461-464, 1978.

[88] Seung, H. S., and H. Sompolinsky. Simple models for reading neuronal population codes. *Proc Natl Acad Sci U S A* 90:10749-53, 1993.

[89] Shoham, S. *Advances towards an implantable motor cortical interface*. Ph.D. dissertation. Dept. of Bioengineering. University of Utah, 2001.

[90] Shoham, S., M. Fellows, and R. Normann. Robust, automatic spike sorting using mixtures of multivariate t- distributions. *J Neurosci Methods*:, accepted, 2003.

[91] Simoncelli, E. P., and D. J. Heeger. A model of neuronal responses in visual area MT. *Vision Res* 38:743-61., 1998.

[92] Snider, R. K., and A. B. Bonds. Classification of non-stationary neural signals. *J Neurosci Methods* 84:155-66, 1998.

[93] Snyder, D. L., and M. I. Miller. *Random point processes in time and space*. Springer texts in electrical engineering. New York: Springer, 1991.

[94] Stanley, G. B., F. F. Li, and Y. Dan. Reconstruction of natural scenes from ensemble responses in the lateral geniculate nucleus. *J Neurosci* 19:8036-42, 1999.

[95] Stuart, G., N. Spruston, B. Sakmann, and M. Hausser. Action potential initiation and backpropagation in neurons of the mammalian CNS. *Trends Neurosci* 20:125-31., 1997.

[96] Terzuolo, C. A., and T. Araki. An analysis of intra versus extracellular potential changes associated with activity in single spinal motoneurons. *Ann NY Acad Sci* 94:547-558, 1961.

[97] Trontelj, Z., V. Jazbinsek, S. N. Erne, and L. Trahms. Multipole expansions in the representation of current sources. *Acta Otolaryngol Suppl* 491:88-92; discussion 93, 1991.

[98] Tuckwell, H. *Introduction to theoretical neurobiology*, 2. New York: Cambridge University Press, 1988.

[99] Warland, D. K., P. Reinagel, and M. Meister. Decoding visual information from a population of retinal ganglion cells. *J Neurophysiol* 78:2336-50, 1997.

[100] Wessberg, J., C. R. Stambaugh, J. D. Krallk, P. D. Beck, M. Laubach, J. K. Chapin, J. Kim, S. J. Biggs, M. A. Srinivasan, and M. A. L. Nicolelis. Real-time prediction of hand trajectory by ensembles of cortical neurons in primates. *Nature* 408:361-365, 2000.

[101] Windham, M., and A. Cutler. Information ratios for validating mixture analysis. *Journal of the American Statistical Association* 87:1188-1192, 1992.

[102] Yao, D. The theoretical relation of scalp Laplacian and scalp current density of a spherical shell head model. *Phys Med Biol* 47:2179-85, 2002.

[103] Zhang, K., I. Ginzburg, B. L. McNaughton, and T. J. Sejnowski. Interpreting neuronal population activity by reconstruction: unified framework with application to hippocampal place cells. *J Neurophysiol* 79:1017-44, 1998.

[104] Zouridakis, G., and D. C. Tam. Identification of reliable spike templates in multi-unit extracellular recordings using fuzzy clustering. *Comput Methods Programs Biomed* 61:91-8, 2000.